An Efficient Beam Steerable Antenna Array Concept for Airborne Applications

Hadi ALIAKBARIAN [1,3], Ewald VAN DER WESTHUIZEN [2], Riaan WIID [2], Vladimir VOLSKIY [1], Riaan WOLHUTER [2], Guy A. E. VANDENBOSCH [1]

[1] ESAT-TELEMIC, KU Leuven, Kasteelpark Arenberg 10 3001, Leuven, Belgium
[2] E&E Engineering Dept., Banghoek Road, Stellenbosch University, Stellenbosch, 7600, South Africa
[3] Dept. of ECE, K.N.Toosi University of Technology, Tehran, Iran

h.aliakbarian@ieee.org, ewaldvdw@sun.ac.za

Abstract. *Deployment of a satellite borne, steerable antenna array with higher directivity and gain in Low Earth Orbit makes sense to reduce ground station complexity and cost, while still maintaining a reasonable link budget. The implementation comprises a digitally beam steerable phased array antenna integrated with a complete system, comprising the antenna, hosting platform, ground station, and aircraft based satellite emulator to facilitate convenient aircraft based testing of the antenna array and ground-space communication link. This paper describes the design, development and initial successful interim testing of the various subsystems. Due to the increase in signal level, our two-element prototype raises the signal-to-noise ratio (SNR) by about 3 dB which is corresponding to a more than 10 times better bit error rate (BER).*

Keywords

Space deployed phased array antenna, beam steering, DSP software defined radio modem, embedded FPGA channel coding.

1. Introduction

One of the best methods to improve the link budget of a Low Earth Orbit (LEO) satellite or an airborne system is to use an expensive tracking antenna system on the ground station. On the other hand for environmental monitoring purposes, it is commonly required that such stations be deployed over a large area and in significant numbers, with small size and low cost. In such situations, the alternative way is to transfer tracking capability to the airborne or satellite borne side of the link.

It would, therefore, be greatly advantageous to use a fixed antenna with wider polar radiation characteristics, but lower associated gain [1]-[3]. This however, implies a higher antenna gain for the satellite, if the power budget is to remain. It should also be steerable, to cater for the greatly varying overflight geometry [4]-[5].

These characteristics are in line with the research objectives of the ESAT-TELEMIC division of the Dept. of Electrical Engineering, of the Katholieke Universiteit Leuven, Belgium. This group is developing advanced techniques for the design of electronically beam steerable antenna arrays, intended for satellite deployment. Directivity and associated higher gain, together with convenient steerability, will allow specific ground stations to be scheduled during satellite overflight with improved link budget, compensating for a fixed, more omnidirectional ground station antenna.

The project is carried out in partnership with the Dept. of Electrical and Electronic Engineering of Stellenbosch University, South Africa, who is developing the rest of the LEO satellite payload, ground station and accompanying ground-space communications link. Ground station coordinates and a per station communications schedule will be uploaded to the satellite via the telecommand link. Satellite position and orientation information will be made available from the satellite bus, in order to enable beam steering and aiming of the antenna axes towards the appropriate ground station.

The purpose of this paper is to report on the development of the communications link, Steerable Antenna Array (SAA) and the calibration method. Some initial test results are also presented; using an aircraft based satellite emulator (ASE) [6]. The rest of the paper is structured as follows. An overview of the systems design is presented in Section 2, followed by an overview of the various subsystems and their functionality, in Section 3. The satellite payload design is also covered in Section 3, with Section 4 presenting a brief review of the communications link and protocol implementation. The ground station re-uses much of the space segment embedded design, but not being restricted to space qualified hardware, and also utilizes some more standard submodules. The configuration thereof is discussed in Section 5. Evaluation and test results were obtained from both simulations and an actual flight simulator. These are presented in Section 6. Section 7 contains a summary of the work performed, and actions planned for the immediate future are discussed in Section 8.

2. System Description

The concept behind the proposed system is simply shown in Fig. 1 and can be summarized as follows: To enable widespread rollout of a terrestrial environmental data acquisition network via a LEO satellite, it is a requirement that ground stations be of a relatively straightforward and low cost design. They might also very likely require deployment in areas without any power or communications infrastructure and apart from any licensing issues, this will constrain transmitter power. This dictates against the use of expensive and power hungry tracking antennas. As a consequence, the link budget is influenced negatively.

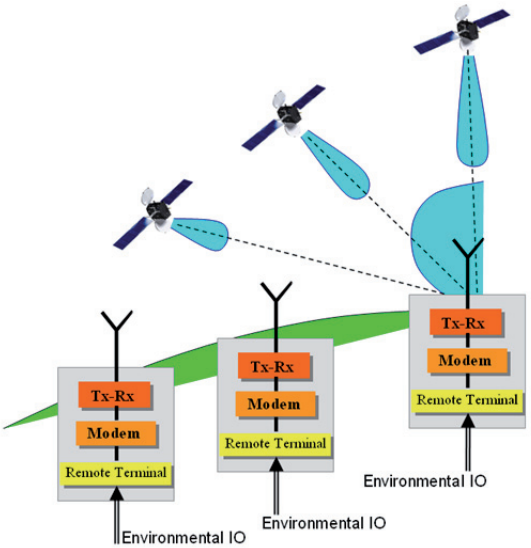

Fig. 1. Ground-Space System Configuration.

The solution determined is to use fixed, more omnidirectional antennas on the ground and a higher gain electronic beam steerable tracking antenna on the satellite. The overflight time window for a typical LEO orbiting at 500 – 600 km, is limited and in the order of 10-12 minutes max. During this time the satellite–ground station distance and consequently the link budget, varies greatly. Detailed link budget calculations are given in [7], resulting in a receiver sensitivity of -110 dBm being chosen as a design specification. A QPSK demodulator requires an input SNR (Eb/No) of 10.5 dB to achieve a BER of 10^{-6} [8]. If the maximum volume of data has to be uploaded during this time, it is vital that the communications time window be utilized to the maximum. This entails that the ground station is kept in the space antenna's maximum gain angular segment for as long as possible and that beam steering is done to achieve this. Mechanical steering is certainly possible, but carries a mass, reliability and cost penalty in space. It is far more attractive to apply electronic beam steering as an alternative. An original realization of such a telecommunication system, including complete hardware and all necessary software, implementing a simple and original digital beam steering, is explained in Section 3 in full detail. A basic two-element array is chosen to give a proof of concept for the final larger array.

A method to ensure fair scheduling of ground station servicing, has been compiled as another part of the overall project. The schedule will take the satellite orbital characteristics and ground station positioning into account, before determining optimum time windows for ground node data uploads. This schedule is uploaded to the satellite via normal mission control telecommands. Ground stations are then tracked during overflight, taking their geographical position and satellite flight parameters into account to feed steering commands to the SAA. The major components in this configuration are, therefore, the ground stations, satellite platform connected to the satellite bus, and communications link with the two ground-space constituent components and incumbent protocol. Due to the expense of actual space qualified hardware, an original and efficient interim subsystem was introduced to facilitate convenient testing on a relatively low flying aircraft. This subsystem, the Aircraft Satellite Emulator (ASE), acts as a translator between the satellite bus and aircraft avionics system, to emulate satellite flight characteristics as far as the payload is concerned (Section 3.3).

3. Subsystem Design

Flight segment consists of two main parts, the communications payload (Fig. 2) and the aircraft satellite emulator (ASE), discussed later in Section 3.3.

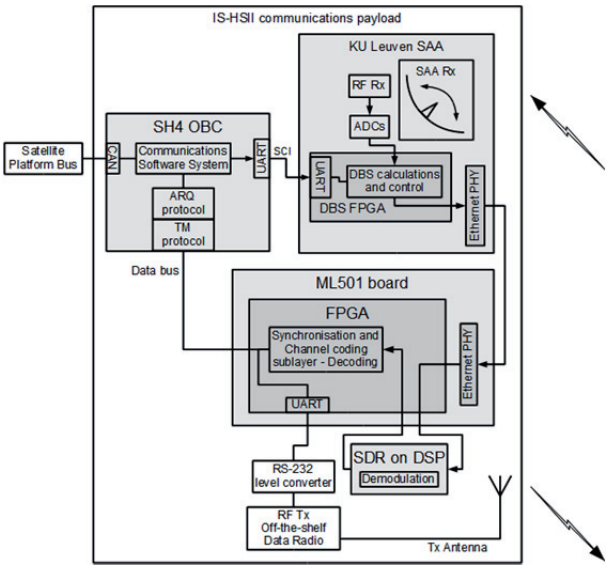

Fig. 2. Satellite payload system block diagram.

3.1 Communication Payload Design

The payload comprises the Hitachi SH4 space hardened on-board computer, a Xilinx ML501 Virtex-5 Evaluation Board, a Freescale DSP56311EVM Board, an off-the-shelf Digi XTend OEM RF Module and antenna (downlink) and the SAA (up-link). Its interfaces are compatible with typical satellite bus and power infrastructure. Note that in further prototypes, the plan is to implement beam

steering in both airborne transmitter and receiver, embedded in one array.

To connect SAA to the payload, two separate interfaces, UART command interface and the Ethernet digital data interface, are used. The UART command interface is used to control the SAA with respect to directional steering and capturing of diagnostic data. It is connected to the On-Board Computer (OBC), which issues the control commands. The Ethernet interface is used to transfer the sampled quadrature baseband signal from the SAA to the SDR modem for demodulation.

3.2 SAA Design

A. Antenna, RF and baseband

The antenna array prototype is composed of the antenna elements, RF section, baseband section, and the digital beam forming part implemented in FPGA. The schematic drawing of the RF and antenna front end of the array is shown in Fig. 3(c). The RF signal is received by each of the antenna elements and then transferred to the RF and baseband board, respectively, and is finally sent to the FPGA board as in-phase and quadrature components. After digital beam steering, I and Q signals are transferred to the FPGA expansion board.

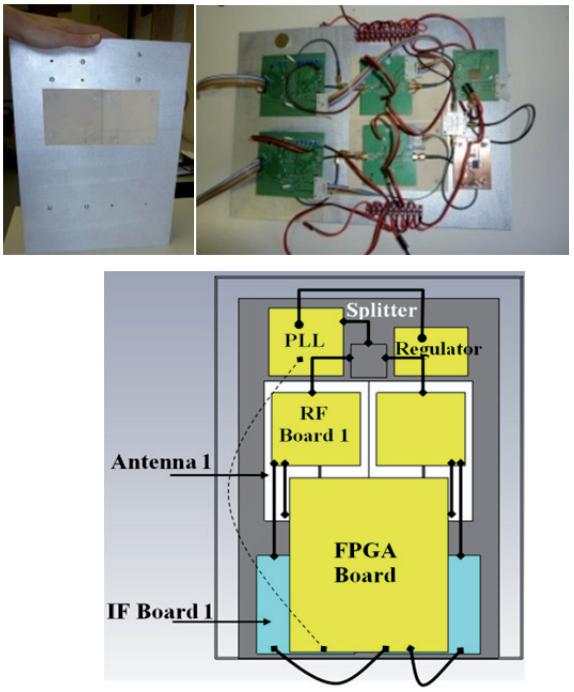

Fig. 3. 1×2 array antenna (a) standing on a table, (b) open from the back, (c) schematic (in CST).

The antenna element, used in the system, is a circularly polarized (CP) aperture coupled patch antenna fed by a rotated microstrip line through a crossed aperture as shown in Fig. 4(a). It is designed based on the work by Kim et al. [9].

As shown in Fig. 4(a), the microstrip feed line covers 270° of a complete tour in order to excite all four branches of the crossed slot with approximately the same magnitude, but with a progressive 90° phase shift. The radius of the rotating feed determines this phase difference. Each arm of the curved feed is designed to be approximately λ/4. The straight end part of the feed line, named L_{os}, is used for matching. The -10 dB return loss bandwidth of the element is 20 % (from 2.2 to 2.7 GHz but the 3 dB axial ratio bandwidth of the antenna is 114 MHz, i.e. 4.6 %. The main reason of this limitation is the change of electrical lengths of the feeding arms. The antenna is fabricated by using a RO4003 substrate and superstrate and an 8 mm air gap in between, as illustrated in Fig. 4(b). The thicknesses of the substrate and superstrate are 0.813 mm and 1.5 mm, respectively.

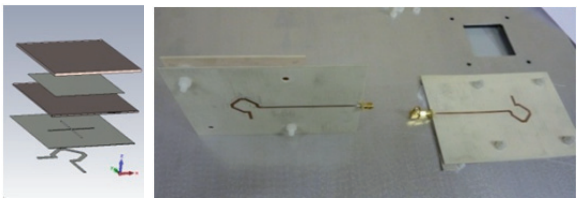

(a) (b)

Fig. 4. (a) Different layers of the final CP element. (b) Fabricated and mounted element.

The measurement results of the single element match almost perfectly with the simulation results in CST [10] Microwave Studio, as seen in Fig. 5. The measurement of the Circular Polarization (CP) performance of one of the manufactured antennas is sketched in Fig. 6 in the φ = 90 degree plane. The asymmetry in the CP performance of the antenna is due to the unsymmetrical feed line and the change of the current amplitude as it proceeds to the next coupling location.

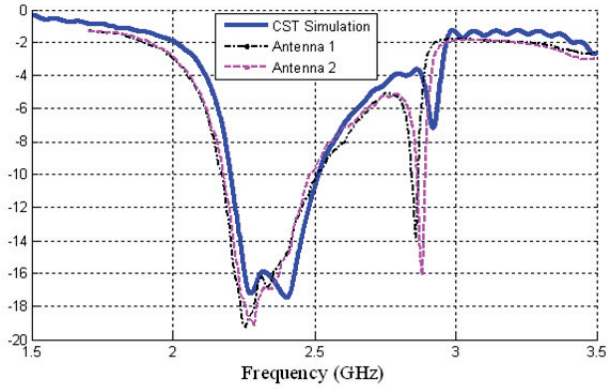

Fig. 5. Simulated and measured return loss of the antenna (S_{11}) in dB .

The RF signal received from the antenna is first amplified using RFMD's LT3866 low noise amplifier (LNA) with 26 dB gain. The RF is then directly converted to quadrature and in-phase components of the baseband signal using LT5575 from Linear Technology. The advantages and drawback of the direct conversion architecture has been discussed in [11] in details. A PLL350-2444 phase-locked loop from RFMD, working between 2344 and 2544 MHz with a 250 kHz frequency step, is used in the local oscillator (LO) board.

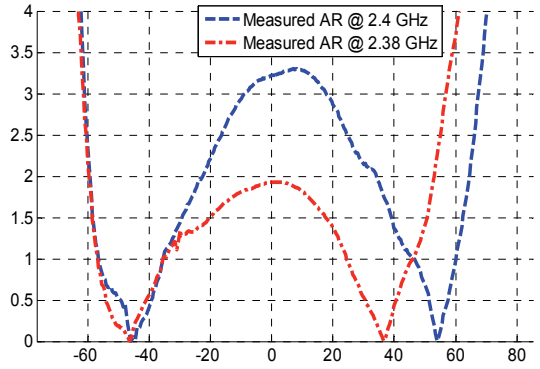

Fig. 6. The measured axial ratio (AR) of the antennas at both 2.38 and 2.4 GHz in the plane φ=90°.

The IF board has been designed to amplify, filter, and digitize the baseband signal and then send it to the FPGA. A newly released dual match bandpass filter from Linear Technology, LTC6602, which includes two parallel programmable gain amplifiers (PGAs), is ideal for the differential I and Q output signals. The gain of the PGAs can be adjusted between 0 to 30 dB. The embedded bandpass filter is also programmable, the lower frequency from 4 to 40 kHz and the upper from 90 to 900 kHz. The use of the Dual-Matched BPF is essential because of the high frequency leakage from the FPGA 12.5 MHz clock. This leakage is highly undesirable for the low level signal. Afterwards, the signal is fed to the 12-bit serial 2.2 MSps LTC1402 analog-to-digital converter (ADC) from Linear Technology. The ADC is controlled by the FPGA using the SPI interface.

B. Element Factor and Array Factor

From antenna theory, the radiation pattern of an antenna array (AP) can be calculated by multiplying the array factor (AF) and the element factor (EF) shown in (1) for a simple one dimensional array.

$$AP(\theta) = EF(\theta).AF(\theta) = EF(\theta).\sum_{i=1}^{n} w_i e^{-j(kx_i \sin(\theta)+\xi)} \quad (1)$$

where w_i is the weight factor, x_i is the position of the i[th] element, and ξ is the applied phase shift between elements. For an ideal array, ξ determines the direction of the main beam from $k.d.sin\ (\theta_{dir})$ where θ_{dir} is the direction of beam, d is the distance between elements and k is the free space propagation constants. Unfortunately due to the effect of EF, the real steered angle of the antenna array is not only decided by θ_{dir} and there will be an error which can be compensated as will be explained in Section 5.

C. Mutual Coupling

If coupling between adjacent elements in an antenna array is significant, its performance degrades and simple array theory of (1) is not valid anymore. In order to investigate this effect, two antenna elements placed 0.82 λ from each other are simulated full wave by using CST. This distance is a compromise between mutual coupling and steering capabilities. It is seen in Fig. 7 that the mutual coupling is around -28 dB in the working frequency band. The return loss is largely unaffected. Unfortunately the element radiation pattern is rotated 6 degrees due to the mutual coupling, as illustrated in Fig. 8. The radiation pattern of the second element is identical but mirrored. This considerably complicates the accurate beam steering. The effect of this distortion on the steering will be discussed in Section 5. Nevertheless, since symmetry is still present in the array, it will show up in the radiation patterns. Fig. 9 for example demonstrates the full wave CST simulation of the array with anti-phase excitation. As expected the radiation pattern has a deep null at boresight.

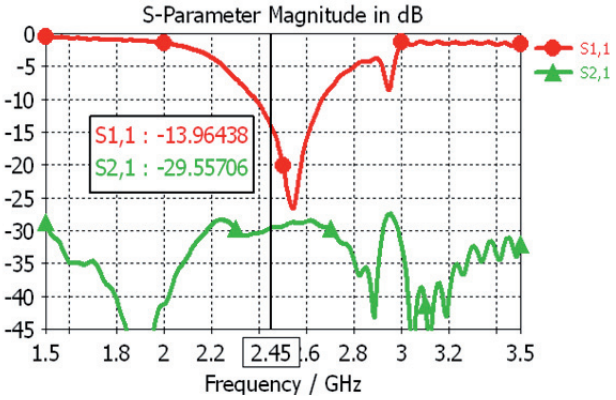

Fig. 7. Return loss and mutual coupling.

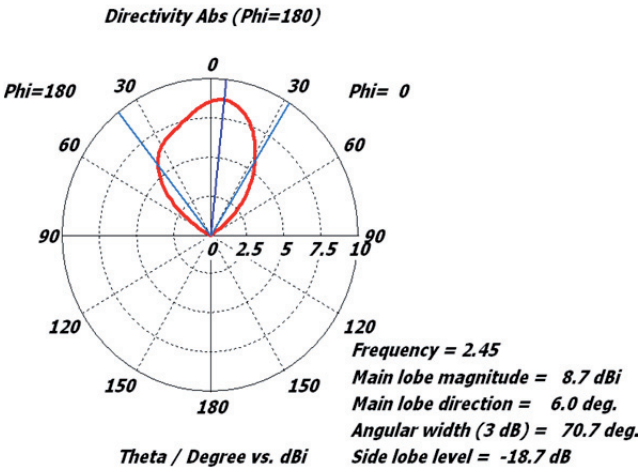

Fig. 8. Rotated radiation pattern of a single element in the φ=90° plane.

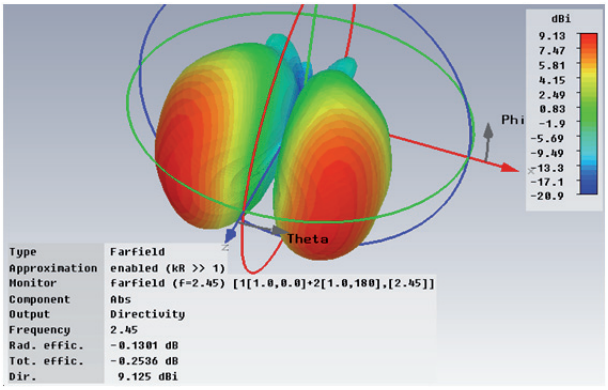

Fig. 9. Radiation pattern of the array with 180° phase shift (anti-phase excitation).

D. Digital Beam Steering Design

The VHDL code mimics a combination of a phase shifter and a summation circuit in the Field Programmable Gate Array (FPGA) environment. Previously the circuit was implemented in an analog way [4]-[5]. The schematic of the digital beam steering system is shown in Fig. 10. It controls all elements including the Phase Locked Loop (PLL). The digital data from the Analog to Digital Converter (ADC) on the baseband board are received by the FPGA board. Then two virtual phase shifters are shifting the phase of the data based on the commands received from the OBC via the Universal Asynchronous Receiver/Transmitter (UART). The phase shifter uses the matrix relation in (2) to change the phase and amplitude of the I_0 and Q_0 signal by the factor a and the phase ξ as explained in [4] in details.

$$\begin{bmatrix} I_0' \\ Q_0' \end{bmatrix} = a \begin{bmatrix} \cos(\xi) & \sin(\xi) \\ -\sin(\xi) & \cos(\xi) \end{bmatrix} \begin{bmatrix} I_o \\ Q_o \end{bmatrix}. \tag{2}$$

This matrix calculation is used to produce the phase for each signal path. A PicoBlaze controller receives the matrix data from the UART and sends them to multipliers embedded in the phase shifters. Finally, the phase shifted signals are summed and sent to the output. We have proposed to modify this matrix and add the imbalance effect to it in order to simplify its function as discussed in the following.

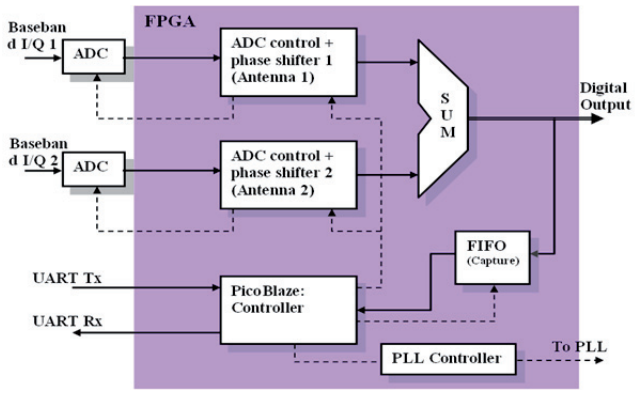

Fig. 10. Schematic of digital beam steering system.

Calibration of the array is performed by capturing raw data samples from each array element and sending the data to the OBC for calculation of the I/Q imbalance compensation values. There are different sources of imbalance, not only between the antenna elements but also between the I and Q signals of each element. The latter is mainly due to imbalances in the amplifiers, filters and components on the baseband board. A simple procedure implemented in the OBC removes all imbalances during the calibration phase. Equation (3) introduces the transfer matrix required for that.

$$\begin{bmatrix} I_0' \\ Q_0' \end{bmatrix} = M \times \begin{bmatrix} \cos(\xi) & \sin(\xi) \\ -\sin(\xi) & \cos(\xi) \end{bmatrix} \begin{bmatrix} I_0 \\ Q_0 \end{bmatrix}, \tag{3}$$

$$M = a_0 \begin{bmatrix} \cos(\theta_\Delta) & \sin(\theta_\Delta) \\ -\sin(\theta_\Delta) & \cos(\theta_\Delta) \end{bmatrix} \times \begin{bmatrix} \beta & 0 \\ \beta\tan(\varphi) & 1/\cos(\varphi) \end{bmatrix}.$$

Here, β and φ are the amplitude and phase imbalances between the I and Q component of one element, respectively, and a_0 and θ_Δ are the amplitude and phase imbalances between the I components of antenna 1 and antenna 2, respectively. The same concept is easily applicable to a higher number of elements. Here, a_0 and θ_Δ can be considered as the amplitude and phase of w_i in (1).

3.3 Emulation Platform

The function of the aircraft satellite emulator (ASE) is to emulate the behavior of a real satellite and its subsystems, for purposes of aircraft based fight testing of the payload [6]. The schematic of the ASE is shown in Fig. 11. It consists of three sections, namely the avionics telemetry interface, the ASE-to-payload interface and the ASE software running on an industrial PC. The avionics telemetry interface collects data packets containing aircraft position and orientation information. The ASE-to-payload interface conforms to the Controller Area Network (CAN) bus standard used by the satellite constructor, SunSpace (SSIS) [12]. To the payload it would appear as if it is connected to an actual SunSpace satellite. The ASE gains access to the CAN bus via a USB-CAN adaptor module. The payload on-board computer (OBC) accesses position and orientation information of the emulated satellite via CAN bus telemetry requests.

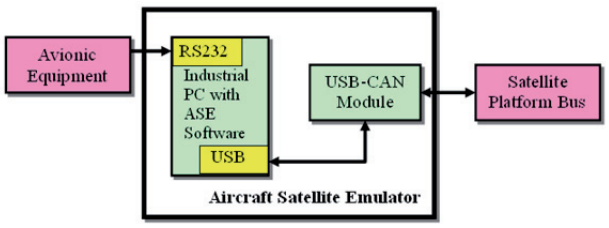

Fig. 11. Aircraft Satellite Emulator block diagram.

4. Payload Communications Link and Protocol Layers

The application layer, transport layer, data link layer and physical layer are the four layers of the Open Systems Interconnect (OSI) model used to realize the communications stack [13]. The communications software system in the application layer enables link acquisition by the payload and is driven by a schedule which determines the ground station communication time and period. It also controls the real-time steering of the SAA, directing the antenna to a scheduled ground station. High-level ground station requests, e.g. file transfers, are handled on a client-server basis. The communications software system transfers data by reading and writing to the transport layer interface. An automatic repeat-request (ARQ) protocol in the

transport layer adds reliable file transfer to the communications system via segmented, re-transmittable data packets. The data link layer transfers fixed data frames between the payload and ground segment and can detect and possibly correct errors that might occur in lower layers. It comprises the two sub-layers based on standards established by the European Cooperation for Space Standardization (ECSS) [14]. The telemetry (TM) transfer frame protocol, located in the data link protocol sub-layer, is designed for space data links and connects at a higher level to the transport layer. The synchronization and channel coding sub-layer is responsible for synchronization and error control coding and connects to the physical layer. Forward error correction (FEC) is implemented to achieve an effective coding gain over the noisy channel. The physical layer consists of an SDR modem used for demodulating the signal received by the SAA (up-link), and an off-the-shelf Digi XTend OEM RF Module used as down-link transmitter. The SDR modem uses differentially encoded QPSK as a modulation scheme. The application layer, transport layer and data link protocol sub-layer are all implemented in the OBC. The synchronization and channel coding sub-layer is implemented on a Xilinx Virtex-5 FPGA. The SDR modem is implemented on a Freescale DSP56321 digital signal processor. A summary of the protocol layers, protocols and their function is given in Tab. 1.

Layer		Protocol or Software System	Function
Application Layer		Communications Software System	Schedules and initiates comms
Transport Layer		ARQ methodology	Ensures reliable file transfer (re-transmittable packets)
Data Link Layer	Data Link Protocol	TM Protocol	Fixed frame transfer and error detection
	Channel Coding and Synchronization	FEC (e.g. BCH or LDPC)	Error detection and correction
Physical Layer		SDR modem (DQPSK)	Baseband modulation

Tab. 1. Summary of protocol layers, protocols used and functional description thereof.

5. Tests and Measurements

5.1 ASE Testing

Tests in the laboratory environment with a flight simulator were performed to ensure that the OBC is able to control the SAA correctly. The flight simulator generates real-time flight data which are sent to the ASE, which in turn makes the aircraft position and orientation available to the payload OBC via the CAN bus. As the OBC requests new flight data from the ASE via telemetry requests, the OBC is able to calculate the required steering angles in order to point the SAA to the currently scheduled ground station. The steering angles are converted to multiplier values, which are programmed into the phase shifters to enable beam steering.

In this simulated test scenario, the aircraft flies directly over a ground station in a simulated environment, as illustrated in Fig. 12, and the signal received by the aircraft is calculated based on our measured SAA performance. As the aircraft approaches the ground station, the nadir angle decreases. As soon as the aircraft crosses the zenith point, there is a 180° jump in rotation angle. The ideal simulation results for a 1×2 array of isotropic elements are shown in Fig. 13(a). The signal level is maximum when the aircraft is on zenith point and it decreases when it goes further from the point. The results obtained with the radiation pattern measurement of the uncompensated array of patch elements are shown in Fig. 13(b). Simulations show that the bottom plot in Fig. 13(b) is an acceptable approximation of the uncalibrated radiation pattern of the array.

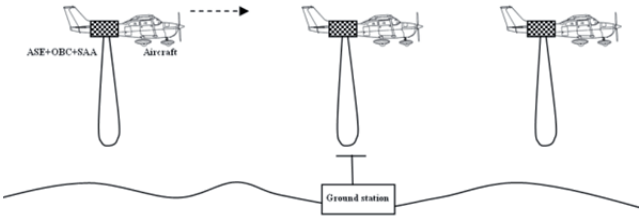

Fig. 12. ASE test scenario.

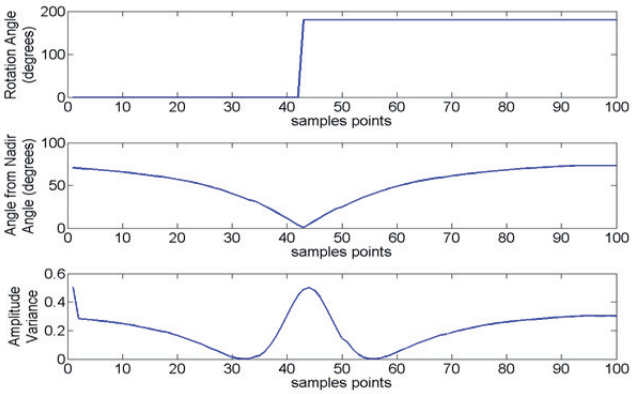

(a) Simulation results for an ideal array.

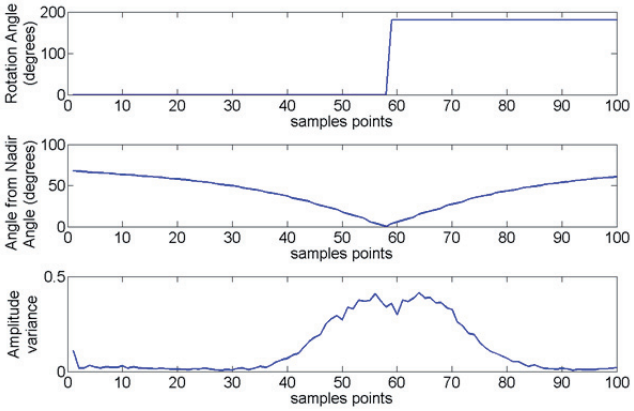

(b) Measured results of an uncompensated array.

Fig. 13. Results of the scenario of Fig. 12.

5.2 Modem Testing

The bit error ratio of the SDR modem was calculated by performing unit tests on the modem subsystem with a known pseudo-random noise sequence. Fig. 14 shows two sets of measurements with their accompanying quadratic fittings. The first measurement set was done by removing all frequency and phase tracking loops and the timing error detector from the demodulator. The demodulator was then fed with a perfectly symbol-aligned signal, modulated with a known pseudo-random bit sequence and then corrupted with additive white Gaussian noise (AWGN). The measured bit error ratio of the demodulated output is plotted with red dots.

The second measurement set was done with the frequency and phase tracking loops and timing error detector included in the demodulation routine. The demodulator was fed with the same known pseudo-random noise sequence as explained in the previous paragraph but with the message signal now placed at an offset frequency within the trackable range of the frequency and phase tracking loops. Again the bit error ratio of the demodulated output was measured. It is plotted with blue dots.

An increase in the bit error ratio occurred for the second measurement set. Reasonable performance is maintained, but with the added ability to track changes in frequency and phase at the expense of losing some reliability. The ability to compensate for changes in frequency and phase ensures that the modem is able to function in an environment where the Doppler Effect is present, as is the case in LEO satellite communications. More details regarding the modem tests can be found in [15].

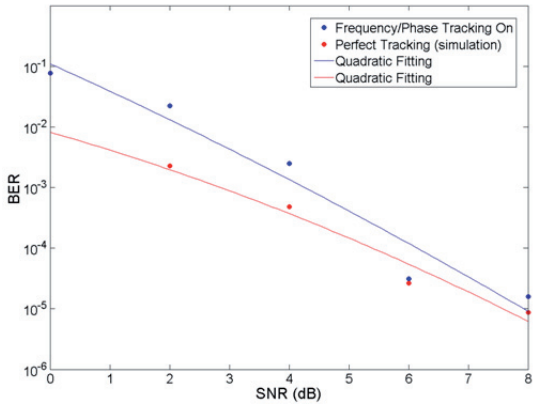

Fig. 14. SDR modem BER versus SNR.

5.3 Digital Beam Steering Functionality

The antenna has been tested in the anechoic chamber of Stellenbosch University, as pictured in Fig. 15. The radiation pattern was measured with a vertically polarized ridged horn antenna. In the first stage, the captured signal data are used to calibrate the array. As discussed earlier, the I and Q amplitude and phase imbalance can then be compensated by using (3).

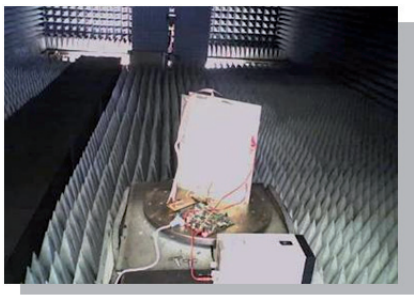

Fig. 15. Antenna rotated to -30° in anechoic chamber and beam also rotated to -30°.

To compensate the I and Q imbalance, imbalance factors β and φ can be determined by using an FFT technique. This method is based on the baseband signal as introduced in [16], [17]. The real I and Q signal can be written as follows:

$$Sig = I + jQ = \cos(\omega t) + j\beta\sin(\omega t + \varphi) = e^{-j\omega t}W_p + e^{+j\omega t}W_N \quad (4)$$

where β is introduced in (3), ω is the baseband frequency which is the difference between the RF and the LO frequency. On the right side of the equation, the first term, W_P, represents the main desired signal translation, while the second term, W_N, represents an undesired image frequency component. A balanced I and Q sine signal delivers only the main component at the corresponding frequency ω, while an imbalanced one also delivers a small image component at the image frequency ($-\omega$). Measuring the main and the image component, we are able to determine β and φ by using

$$\beta \approx \frac{1 + \mathrm{Re}\left(\frac{W_P^*}{W_N}\right)}{1 - \mathrm{Re}\left(\frac{W_P^*}{W_N}\right)}, \quad \varphi \approx 2\arctan(-\mathrm{Im}(W_P^*/W_N)) \quad (5)$$

Therefore to compensate the signal, at each angle 64 data samples are captured from each element using a carrier at 2.44 GHz. The captured baseband signal, which should be a sine at a few tens of kHz, is shown in the constellation diagram (i.e. Q versus I component) of Fig. 16. The ideal I and Q diagram is a perfect circle. Imbalances lead to an elliptical shape. In this figure, the outer group of ellipses is representing the captured raw imbalanced signal, while the interior quasi-circles are the result after balancing.

Thus, in order to measure W_P and W_N, at different rotation angles from -60 to 60 degrees, an FFT is applied to the captured signal of each element to get the frequency content of the signal, shown in Fig. 17 for one of the elements. The Z-axis, Y-axis and X-axis are the FFT amplitude, frequency and rotation angle of the antenna, respectively. The main component of the FFT is centered around +48 kHz while the image component of the FFT, resulting from the imbalance, is visible around -48 kHz. The interior group of circles in Fig. 17 depicts the signal after compensation based on the data obtained from the FFT.

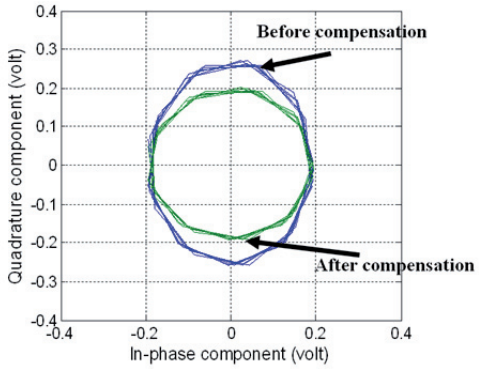

Fig. 16. Imbalance compensation diagram, the interior circles (green) correspond to the uncompensated signal and the outer circles (blue) correspond to the compensated signal.

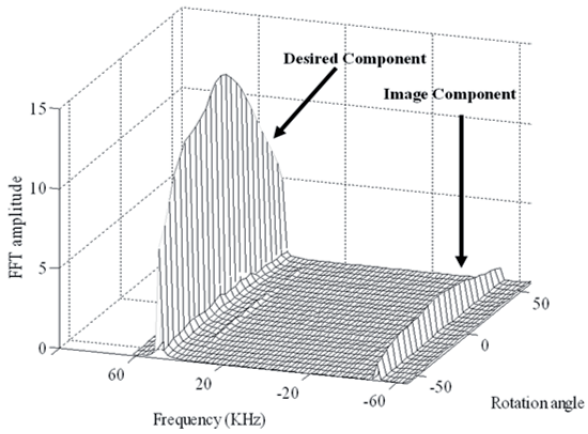

Fig. 17. FFT over the imbalanced captured I and Q signal.

After the calibration step, radiation patterns were measured. This is done by observing the digital voltage captured in the FPGA, while changing the angle of the antenna, with the phase shifters set to certain pre-calculated values corresponding to a specific beam steering angle. Steering angles 0° and -30° were considered. The corresponding phase shift between elements was calculated based on

$$AP(\theta,\phi) = EF_1(\theta,\phi)e^{-jkd\sin(\theta_{dir})} + EF_2(\theta,\phi) \qquad (6)$$

assuming that the antenna element radiation patterns are exactly the same. The measured result and full wave simulations with CST are shown (in normalized scale) in Fig. 18. The simulation results are in very good agreement with the measurement results. When there is no phase difference between the elements, i.e. for 0° steering, the maximum reception is indeed at 0°. However, it is seen that the radiation pattern is steered to -20° instead of -30°, even with the calibration in place. This is mainly the effect of two factors, element factor (as already mentioned in Section 3.2.b) and mutual coupling between the elements which deforms the amplitude and phase of the single element radiation patterns (as explained in Section 3.2.c). There is also a considerable sidelobe at +35°. This is mainly due to the fact that the inter-element distance is 0.82 λ, which brings the first grating lobe close to the visible range. This grating lobe becomes as strong as the main lobe when the beam is rotated out of ±36° range.

Simulations show that the effect of element factor on the steering is more severe and the mutual coupling error is less important. The first effect can be seen in Fig. 19. It is described in full detail, together with a technique to correct it in [18]. This technique has been applied here. The calibration data can be determined by adjusting the calibration matrix in an appropriate way and taking the real angle of the beam into account. For instance, in order to steer the beam to -20 degrees, the calibration matrix for -30 degrees should be used.

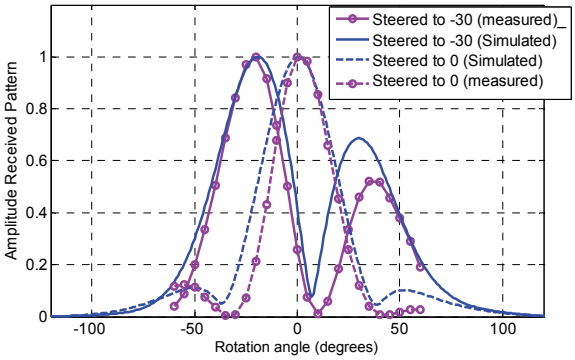

Fig. 18. Normalized radiation pattern rotated to 0° and -30°: full wave simulation versus measurement.

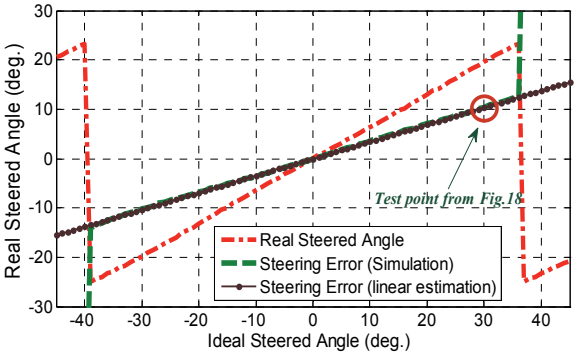

Fig. 19. Steering error correction: real steered angle vs. ideal steered angle and the calculated error.

6. Conclusion and Future Work

In this paper a LEO satellite borne beam steerable antenna array and the required surrounding systems infrastructure were described. The aim of the system is to reduce ground station cost, while still maintaining a good link budget and, as a result, a good volumetric data throughput. Up to this point, all tests on the different subsystems have been successful and design objectives have been met. Further verification of overall performance entails practical testing of the entire system in an operational environment. A light aircraft test will provide useful information regarding operational capability and any design, or construction changes required for the actual space flight model.

Acknowledgements

The authors would like to thank the Department of Economy, Science and Innovation (EWI) of the Flemish government for its financial support within the frame-work of the IS-HS project.

References

[1] COLANTONIO, D., ROSITO, C. A spaceborne telemetry loaded bifilar helical antenna for LEO satellites. In *Proc. SBMO/IEEE MTT-S IMOC*. Brazil, Nov. 3, 2009, p. 741 - 745.

[2] REZAEI, P., ALIAKBARIAN, H., et al., Beam shaping of turnstile antenna for LEO satellite with genetic algorithm. In *Proc. of 10th MMET Conference*. Dniepropetrovsk (Ukraine), 2004, p. 470.

[3] BALLING, P. Analytical high-efficiency spot-beam model for high throughput satellites. *Radioengineering*, Dec. 2012, vol. 21, no. 4, p. 1078 - 1084.

[4] ALIAKBARIAN, H., VOLSKI, V., VAN DER WESTHUIZEN, E., WOLHUTER, R., VANDENBOSCH, G. A. E. Analogue versus digital for baseband beam steerable array used for LEO satellite applications. In *Proc. of 4th EuCAP*. Barcelona (Spain), 12 - 16 April 2010.

[5] AERTS, W., DELMOTTE, P., VANDENBOSCH, G. A. E. Conceptual study of analog baseband beam forming: design and measurement of an eight-by-eight phased array. *IEEE Transactions on Antennas and Propagation*, 2009, vol. 57, no. 5, p. 1667 - 1672.

[6] KRUGER, I. C., WOLHUTER, R. An aircraft based emulation platform for LEO satellite antenna beam steering. In *Proc. of 5th ICSNC Conference*. Nice (France), 22-27 Aug., 2010, p. 221.

[7] KRUGER I. C. An aircraft based emulation platform and control model for LEO satellite antenna beam steering. *MSc Eng. Thesis*. Stellenbosch University, Stellenbosch (South Africa), 2010.

[8] *Handbook of Satellite Communications.* International Telecommunications Union (ITU), 3rd ed. ISBN: 978-0-471-22189-0.

[9] KIM, H., LEE, B. M., YOON, Y. J. A single-feeding circularly polarized misrostrip antenna with the effect of hybrid feeding. *IEEE Antennas Wireless Propagat. Letters*, 2003, vol. 2, p. 74 - 77.

[10] *CST Microwave Studio 2010*. CST Computer Simulation Technology AG. [Online] Available at: www.cst.com.

[11] RAZAVI, B. Design considerations for direct-conversion receivers. *IEEE Trans. Circuit and Systems-II*, June. 1997, vol. 44, no. 6, p. 428 - 435.

[12] *Sunspace, Innovative Satellite Solutions.* Stellenbosch, South Africa. [Online] Available at: www.sunspace.co.za.

[13] BOTHA, J. S. A reusable signal processing architecture for satellite based communication systems. *M.Sc Eng. Thesis*, University of Stellenbosch, Stellenbosch (South Africa), 2011.

[14] *Space Engineering Standards: Recommendations for CAN Bus in Spacecraft Onboard Applications.* ECSS Standard E-50, May 2005.

[15] VAN DER WESTHUIZEN, E., VAN ROOYEN, G. J. Baseband carrier recovery and phase tracking as a Doppler compensation technique for a zero-IF SDR. In *Proc. of SATNAC'09*. Swaziland, 2009.

[16] VAN ROOYEN, G. J., LOURENS, J. G. A non-iterative I/Q imbalance compensation technique for quadrature mixing receivers. In *Proc. of IEEE WCNM 2005*. China, 23-26 Sept, 2005, p. 598 – 601.

[17] DE WITT J. J. Modeling estimation and compensation of imbalances in quadrature transceivers. *PhD Dissertation*. Stellenbosch University, Stellenbosch (South Africa), 2011.

[18] ALIAKBARIAN, H., XU, H., VANDENBOSCH, G. A. E. Simple technique to predict beam direction based on element pattern and array factor in small- and medium-sized arrays. *IEEE Antennas Wireless Propagat. Letters*, 2012, vol. 11, p. 763 - 766.

About Authors...

Hadi ALIAKBARIAN is an Assistant Professor in K.N.Toosi University of Technology in Iran. He received the B.S and M.S degrees in Electrical and Telecommunication Engineering from the University of Tehran in 2002 and 2005, and the Ph.D degree in Electrical Engineering from the Katholieke Universiteit Leuven (KU Leuven) in 2013. He worked for the microwave laboratory and the Center of Excellence on Applied Electromagnetics at the University of Tehran as an Associated Researcher from 2005 to 2007. His research interests include different aspects of digital and analog beam steering (especially in space conditions), small antennas, UWB antennas, antenna optimization, and EMC problems.

Ewald VAN DER WESTHUIZEN completed his B.Eng (Electronic) degree in 2000 and his M.Sc.Eng in 2003, both at Stellenbosch University. After four years of employment at Amai Technologies and Nellymoser, Inc., he joined Stellenbosch University in 2007 as a Project Engineer and Researcher in DSP and telecommunications.

Riaan WIID received his B.Eng degree in Electrical and Electronic Engineering at the University of Stellenbosch in 2009. From the same university he received his Master's degree with distinction, in Satellite Telecommunications Systems. Here his primary focus was to implement Low-Density Parity-Check (LDPC) forward error correction for a FPGA and firmware based ARQ protocol. This was intended for a Low Earth Orbit (LEO) satellite project, which is a joint effort between the Katholieke Universiteit Leuven and Stellenbosch University. During his Master's degree, he also performed senior mentoring duties for various engineering courses. He is currently doing embedded programming and design in the private sector.

Vladimir VOLSKIY graduated from the Moscow Power Engineering Institute, Moscow, Russia, in 1987. In the same year he joined the division Antennas and Propagation of Radio Waves of the same institute as a researcher. In 1993 he received the degree of Candidate of Science (Ph.D). Since January 1996 he has been a post-doctoral researcher at the ESAT-TELEMIC division of the Katholieke Universiteit, Leuven, Belgium. His main research interests include electromagnetic theory, computational electromagnetics, and modeling and measuring of electromagnetic radiation, including bio-electromagnetics.

Riaan WOLHUTER is a Senior Researcher at the Dept. of Electrical & Electronic Engineering, Stellenbosch University, South Africa, and is involved with the post-grad programme and research in telecommunications. He holds a PhD degree from the same university and is author, or co-

author, of 19 peer reviewed publications. He is a project manager and technical coordinator of 3 current projects in satellite communications development at the Stellenbosch University and manager of the Department's focus area in Advanced Telecommunications. He specializes in Communications Systems Design with emphasis on advanced MAC layer strategies, for telemetry systems in particular. He also serves on the technical and programme committee of several international conferences and acts as a regular reviewer for a number of well-known journals. He is an invited professor at 2 major European universities and participant in a European Framework Programme activity.

Guy A. E. VANDENBOSCH is a Full Professor at KU Leuven. His interests are in the area of electromagnetic theory, computational electromagnetics, planar antennas and circuits, nano-electromagnetics, EM radiation, EMC, and bio-electromagnetics. His work has been published in ca. 185 papers in international journals and has led to ca. 300 presentations at international conferences. Currently, he leads the Working Group on Software within EuRAAP, he holds the position of chairman of the IEEE AP/MTT Benelux Chapter, and is a secretary of the Belgian National Committee for Radio-electricity (URSI). Dr. Vandenbosch is a fellow of the IEEE since January 2013.